

High-order quasi-Helmholtz Projectors: Definition, Analyses, Algorithms

Johann Bourhis, Adrien Merlini, *Member, IEEE*, and Francesco P. Andriulli, *Fellow, IEEE*

Abstract—The accuracy of the electric field integral equation (EFIE) can be substantially improved using high-order discretizations. However, this equation suffers from ill-conditioning and deleterious numerical effects in the low-frequency regime, often jeopardizing its solution. This can be fixed using quasi-Helmholtz decompositions, in which the source and testing elements are separated into their solenoidal and non-solenoidal contributions, then rescaled in order to avoid both the low-frequency conditioning breakdown and the loss of numerical accuracy. However, standard quasi-Helmholtz decompositions require handling discretized differential operators that often worsen the mesh-refinement ill-conditioning and require the finding of the topological cycles of the geometry, which can be expensive when modeling complex scatterers, especially in high-order. This paper solves these drawbacks by presenting the first extension of the quasi-Helmholtz projectors to high-order discretizations and their application to the stabilization of the EFIE when discretized with high-order basis functions. Our strategy will not require the identification of the cycles and will provide constant condition numbers for decreasing frequencies. Theoretical considerations will be accompanied by numerical results showing the effectiveness of our method in complex scenarios.

Index Terms—Boundary element method, electric field integral equation, high-order, quasi-Helmholtz projectors, low-frequency, preconditioning.

I. INTRODUCTION

MODELLING and simulation of electromagnetic scattering from perfectly electrically conducting (PEC) objects can be effectively performed using surface integral equations [1], [2]. Among these formulations, the electric field integral equation (EFIE) is one of the most widely used. This equation is usually solved via the boundary element method (BEM) [3] by approximating the current as a combination of basis functions with a finite support defined on a surface mesh of the object. The accuracy of the method consequently depends on the ability of the mesh and basis functions to respectively describe the surface and the current functional space. Very often, zeroth-order basis functions such as the Rao-Wilton-Glisson (RWG) functions are employed with flat triangular cells [4]. Thus, the mesh density and the functional space discretization are usually increased simultaneously by refining the mesh, which leads to a higher number of cells and basis functions.

Alternatively, high-order mesh and functional space discretizations [5], [6] can be employed to improve the accuracy

without necessarily increasing the mesh density. High-order basis functions also provide a faster convergence to the physical solution when refining the mesh [7], [8]. Nevertheless, despite the use of a more accurate framework, the EFIE suffers from ill-conditioning and loss of significant digits at low-frequency [9].

The stabilization of the EFIE using quasi-Helmholtz decomposition [10]–[13] is well-known, even in the high-order case [14], [15]. It consists in a change of basis that allows to reorganize the system into solenoidal and non-solenoidal contributions and to rescale them appropriately to cure the problematic behavior of the EFIE at low-frequency. However, the construction of the solenoidal basis functions can be burdensome because it requires the identification of the global cycles; a task that might be challenging when modeling complex geometries [9].

More recently, the method of the quasi-Helmholtz projectors has been developed for the RWG case [9]. The method generates orthogonal projectors over the solenoidal and non-solenoidal subspaces from the computation of the Star matrix, without having to explicitly identify the cycles. They are subsequently used to separate and to rescale the different contributions of the EFIE, without further degrading the condition number when increasing the mesh-density [9].

This work proposes for the first time the high-order counterpart of the quasi-Helmholtz projectors for the stabilization of the EFIE when using high-order basis functions. The contribution will first present a general definition of the Star basis functions in high-order that encompasses several choices in terms of basis elements and testing in the charge space. The contribution will then show that the consequential definition of the quasi-Helmholtz projectors is not dependent on any of these specific choices. Finally the new projectors will be used to regularize the electric field integral equation discretized with high-order elements.

This paper is organized as follows. In Section II, we set the background and the notations. In section III, we extend the definition of the quasi-Helmholtz projectors to the high-order framework. We show their completeness to represent the Graglia-Wilton-Peterson (GWP) basis [5] and their uniqueness with respect to the choice of the Star basis, as well as their application to solve the low-frequency breakdown. In section IV, we present the implementation details required to achieve effective algorithms. Finally, section V provides numerical results which validate the preconditioning technique on relevant scenarios. The results of this work were presented in a conference contribution [16] that generalized the preliminary investigations in [17].

J. Bourhis and F. P. Andriulli are with the Department of Electronics and Telecommunications, Politecnico di Torino, 10129 Torino, Italy; e-mail: francesco.andriulli@polito.it.

A. Merlini is with the Microwave department, IMT Atlantique, 29238 Brest cedex 03, France; e-mail: adrien.merlini@imt-atlantique.fr.

Manuscript received August 25, 2023.

II. BACKGROUND AND NOTATIONS

This section will introduce the necessary background material and notation on integral equations and related high-order discretizations. The treatment will be brief and with the primary goal of setting the notations. The interested reader is referred to the more extensive treatments in [5], [7], [18]–[20] and references therein.

Consider the scattering from a PEC object with boundary Γ residing in a homogeneous medium with wavenumber k and characteristic impedance η . The current \mathbf{J} induced on Γ by an incident electric field \mathbf{E}^i can be obtained by solving the EFIE [2]

$$\mathcal{T}\mathbf{J} = -\hat{\mathbf{n}} \times \frac{1}{\eta} \mathbf{E}^i, \quad (1)$$

with

$$\mathcal{T} = jk\mathcal{T}_s - \frac{1}{jk}\mathcal{T}_h, \quad (2)$$

where the vector and scalar potentials are defined as

$$(\mathcal{T}_s\mathbf{J})(\mathbf{r}) = \hat{\mathbf{n}} \times \int_{\Gamma} G(\mathbf{r}, \mathbf{r}') \mathbf{J}(\mathbf{r}') dS(\mathbf{r}'), \quad (3)$$

$$(\mathcal{T}_h\mathbf{J})(\mathbf{r}) = \hat{\mathbf{n}} \times \nabla_{\Gamma} \int_{\Gamma} G(\mathbf{r}, \mathbf{r}') \nabla_{\Gamma} \cdot \mathbf{J}(\mathbf{r}') dS(\mathbf{r}'), \quad (4)$$

and where $\hat{\mathbf{n}}$ is the outgoing normal vector from Γ , ∇_{Γ} is the surface nabla operator, and the Green's kernel is

$$G(\mathbf{r}, \mathbf{r}') = \frac{e^{-jk|\mathbf{r}-\mathbf{r}'|}}{4\pi|\mathbf{r}-\mathbf{r}'|}. \quad (5)$$

The solution \mathbf{J} of (1) lives in the functional space $H_{\text{div}}^{-\frac{1}{2}}(\Gamma)$, for which a well-suited arbitrary order discretization approach is given by the Nédélec's mixed-order div-conforming spaces [19], [20]. These spaces can be generated by different sets of basis functions [5], [18], [21]. In the following, for fixing ideas, we will focus on the Graglia-Wilton-Peterson (GWP) basis function set, but our considerations and findings will apply also to several other bases. The p -th order GWPs are defined as the product of the RWGs (zeroth-order GWPs) with order p shifted Silvester-Lagrange functions [5]. In what follows, we denote by $\{\psi_n^{(p)}\}_{n=1}^{N_p}$ the set of GWP basis functions, where the total number of functions is

$$N_p = (p+1)E_{\text{int}} + p(p+1)C, \quad (6)$$

with E_{int} and C the number of internal edges and cells of the mesh. A detailed definition of these basis functions is omitted here for space limitation, but we refer the reader to [5] and [18].

The space spanned by the GWPs' divergences is included into the space of cell-wise polynomials complete up to order p [6], that is of dimension

$$M_p = \frac{(p+1)(p+2)}{2}C, \quad (7)$$

and that we denote by $\mathbb{P}(\Gamma, p)$ in what follows. We consider on each triangle a set of $\frac{(p+1)(p+2)}{2}$ interpolatory points, which give a total set of points $\{\mathbf{r}_j\}_{j=1}^{M_p}$ for the whole mesh (with overlapping for the points defined on the triangles' boundaries). On these points, we define a Lagrange interpolatory

basis for $\mathbb{P}(\Gamma, p)$ that we denote by $\{\sigma_m^{(p)}\}_{m=1}^{M_p}$. More explicitly we have

$$\sigma_m(\mathbf{r}_j) = \delta_{mj}, \quad (8)$$

with δ_{mj} the Kronecker symbol and σ_m is a piecewise continuous function which is polynomial of degree p on one cell and zero on all the others.

Because of charge neutrality, the total number of degrees of freedom (DoFs) for the divergence space (charge DoFs) is $M_p - N_{\text{bodies}}$ [14], where N_{bodies} is the number of separate connected bodies of the mesh. The GWP space can be decomposed as a combination of non-solenoidal functions, corresponding to the charge DoFs, and a combination of solenoidal (divergence free) functions that complement the charge DoFs.

The GWP functions $\{\psi_n^{(p)}\}$ can be used within a BEM strategy, by approximating the current in (1) as

$$\mathbf{J}(\mathbf{r}) \approx \sum_{n=1}^{N_p} j_n \psi_n^{(p)}(\mathbf{r}) \quad (9)$$

and, after testing (1) with the rotated GWP elements $\{\hat{\mathbf{n}} \times \psi_n^{(p)}\}$, the EFIE yields a matrix system

$$\mathbf{T}\mathbf{j} = \mathbf{e}, \quad (10)$$

with

$$\mathbf{T} = jk\mathbf{T}_s + \frac{1}{jk}\mathbf{T}_h, \quad (11)$$

where

$$[\mathbf{T}_s]_{mn} = \int_{\Gamma \times \Gamma} G(\mathbf{r}, \mathbf{r}') \psi_n^{(p)}(\mathbf{r}') \cdot \psi_m^{(p)}(\mathbf{r}) dS(\mathbf{r}') dS(\mathbf{r}), \quad (12)$$

$$[\mathbf{T}_h]_{mn} = \int_{\Gamma \times \Gamma} G(\mathbf{r}, \mathbf{r}') \nabla_{\Gamma} \cdot \psi_n^{(p)}(\mathbf{r}') \nabla_{\Gamma} \cdot \psi_m^{(p)}(\mathbf{r}) dS(\mathbf{r}') dS(\mathbf{r}), \quad (13)$$

$$[\mathbf{e}]_m = -\frac{1}{\eta} \int_{\Gamma} \mathbf{E}^i(\mathbf{r}) \cdot \psi_m^{(p)}(\mathbf{r}) dS(\mathbf{r}). \quad (14)$$

At low-frequency, the EFIE faces several numerical challenges. First, the EFIE linear system becomes increasingly ill-conditioned for decreasing frequencies due to the frequency ill-scaling of vector and scalar potentials [9]. In particular

$$\lim_{k \rightarrow 0} \text{cond}(\mathbf{T}) = \mathcal{O}(k^{-2}). \quad (15)$$

This ill-conditioning impacts the accuracy of the solution and increases the number of iterations required by iterative solvers. A second numerical challenge is related to the loss of significant digits in the context of finite precision computations when evaluating the right-hand-side \mathbf{e} , the solution \mathbf{j} and the radiated field [9].

Both effects are related to the quasi-Helmholtz decomposition of the current, because solenoidal and non-solenoidal contributions in the EFIE system have different frequency behaviors. By decomposing the source and testing elements into their solenoidal and non-solenoidal components, it is possible to properly rescale these contributions to cure both of these issues. In the zeroth-order case, this strategy can be applied in a particularly effective way by leveraging

quasi-Helmholtz projectors [9]. Differently from other quasi-Helmholtz decompositions such as Loop-Star/Tree and related approaches, this mathematical tool allows for the rescaling of scalar and vector potential without perturbing the other conditioning properties of the equation. The generalization of quasi-Helmholtz projector strategies to the high-order case, however, is far from trivial because of the need for a proper extension of the graph Laplacian matrices [9] to the high-order case. Such a generalization will be the subject of Section III.

III. HIGH-ORDER QUASI-HELMHOLTZ PROJECTORS

In this section we will define high-order quasi-Helmholtz projectors to address the above described low-frequency limitations of the EFIE in the high-order case. From the zeroth-order case [9] we learn that primal projectors can be obtained from a properly chosen *Star matrix*. The problem is that a unique definition of a Star matrix in high-order can be challenging [14]. In this contribution, we will propose one approach to define a Star matrix that, indeed, does not lead to a unique definition. We will equally show in this paper, however, that the corresponding Star (non-solenoidal) projector will be invariant, regardless of the non-uniqueness of the Star definition we will adopt.

A. Construction of the high-order quasi-Helmholtz projectors

Given the coefficients \mathbf{j} of a function expressed as a linear combination of GWP functions, one could think of building a high-order Loop-Star decomposition in the form

$$\mathbf{j} = \Sigma_p \mathbf{s} + \Lambda_p \mathbf{l} + \mathbf{H}_p \mathbf{h}. \quad (16)$$

Similarly to the zeroth-order case Λ_p and \mathbf{H}_p express the local-Loops-to-GWP and global-cycles-to-GWP change of bases, respectively [9]. In the following we will not need an explicit definition of these two matrices and we will not discuss them further. We will only be using the fact that both Λ_p and \mathbf{H}_p contain coefficient representations of solenoidal functions. As pertains to Σ_p , we will refer to this matrix as the high-order *Star matrix*, with an abuse of terminology stemming from the zeroth-order case. Consider now the injective linear function \mathcal{L}

$$\mathcal{L}: \begin{array}{l} \mathbb{P}(\Gamma, p) \longrightarrow \mathbb{R}^m \\ q(\mathbf{r}) \longmapsto \mathcal{L}q \end{array} \quad (17)$$

with $[\mathcal{L}q]_m = \mathcal{L}_m q$. It should be noted that injectivity and linearity imply

$$\mathcal{L}q = 0 \iff q(\mathbf{r}) = 0 \quad \forall \mathbf{r} \in \Gamma. \quad (18)$$

Now we can propose the following general definition for Σ_p

$$[\Sigma_p]_{i,j} = [\mathcal{L} \nabla_{\Gamma} \cdot \psi_i^{(p)}]_j \quad (19)$$

By the construction of Σ_p and because Λ_p and \mathbf{H}_p describe solenoidal functions we get

$$\Sigma_p^T \Lambda_p = \mathbf{0} \quad (20)$$

and

$$\Sigma_p^T \mathbf{H}_p = \mathbf{0}. \quad (21)$$

The above conditions result in that all coefficients of solenoidal functions are in the null-space of Σ_p^T . Also the converse statement, all elements of the null space of Σ_p^T are coefficients of solenoidal functions, is true following from (18) and (19). Since the solenoidal subspace of the GWPs has a dimension $N_p - M_p + N_{\text{bodies}}$ [14], the null-space of Σ_p^T has dimension $N_p - M_p + N_{\text{bodies}}$. As a consequence, the dimension of the range of Σ_p^T , which is also the dimension of the range of Σ_p , equals to $N_p - (N_p - M_p + N_{\text{bodies}}) = M_p - N_{\text{bodies}}$. This fact proves that $[\Sigma_p, \Lambda_p, \mathbf{H}_p]$, a rectangular matrix, has a rank equal to the number of basis functions N_p in (6). This shows that our definition of the high-order Stars Σ_p^T produces a valid complement of the solenoidal subspaces as the columns of $[\Sigma_p, \Lambda_p, \mathbf{H}_p]$ generate the entire GWP space.

We are now ready to define the quasi-Helmholtz projectors. In particular, mimicking the zeroth-order case, define

$$\mathbf{P}_p^{\Sigma} = \Sigma_p \left(\Sigma_p^T \Sigma_p \right)^+ \Sigma_p^T \quad (22)$$

and

$$\mathbf{P}_p^{\Lambda H} = \mathbf{I} - \mathbf{P}_p^{\Sigma}. \quad (23)$$

It should be noted that, because of the orthogonality of the projectors, i.e.

$$\mathbf{P}_p^{\Sigma} \mathbf{P}_p^{\Lambda H} = \mathbf{P}_p^{\Sigma} (\mathbf{I} - \mathbf{P}_p^{\Sigma}) = \mathbf{P}_p^{\Lambda H} \mathbf{P}_p^{\Sigma} = \mathbf{P}_p^{\Sigma} - \mathbf{P}_p^{\Sigma} = \mathbf{0}, \quad (24)$$

and because of completeness of the decomposition, $\mathbf{P}_p^{\Lambda H}$ is the projector in the solenoidal (local and global Loops) subspace.

From the generality of our definition of Σ_p in (19) one could think of obtaining a different set of projectors for each specific choice Σ_p . We will now prove that, instead, the high-order quasi-Helmholtz projectors, with our definition, are invariant under any particular choice of the high-order Star matrix. In particular

Proposition 1. *Consider two different operators \mathcal{L} and $\tilde{\mathcal{L}}$ both satisfying definition and properties in (17) with associated matrices Σ_p and $\tilde{\Sigma}_p$, respectively defined via (19), then there exists an invertible matrix \mathbf{M} so that $\tilde{\Sigma}_p = \Sigma_p \mathbf{M}$.*

Proof. Consider an arbitrary basis $\{b_k\}_{k=1}^{M_p}$ of $\mathbb{P}(\Gamma, p)$. We can then express the divergence of each $\psi_i^{(p)}(\mathbf{r})$ as

$$\nabla \cdot \psi_i^{(p)}(\mathbf{r}) = \sum_{k=1}^{M_p} a_{ik} b_k(\mathbf{r}) \quad (25)$$

with a proper set of coefficients $\{a_{i,k}\}_{k=1}^{M_p}$ for each $\psi_i^{(p)}(\mathbf{r})$. Since both Σ_p and $\tilde{\Sigma}_p$ are defined on the same GWP set $\psi_i^{(p)}(\mathbf{r})$ and assuming, without loss of generality, the same ordering of the basis functions in both cases, from (25) we have

$$\Sigma_p = \mathbf{A} \mathbf{L} \quad \text{and} \quad \tilde{\Sigma}_p = \mathbf{A} \tilde{\mathbf{L}} \quad (26)$$

with $[\mathbf{A}]_{ik} = a_{ik}$, $[\mathbf{L}]_{kj} = \mathcal{L}_j b_k$, and $[\tilde{\mathbf{L}}]_{kj} = \tilde{\mathcal{L}}_j b_k$.

Using the definition, linearity, and injectivity of \mathcal{L} , together with the completeness of the basis $\{b_k\}_{k=1}^{M_p}$, we obtain

$$\begin{aligned} \mathbf{L}^T \mathbf{x} = \mathbf{0} &\Rightarrow \sum_{k=1}^{M_p} (\mathcal{L}_m b_k) x_k = 0 \quad \forall m \\ &\Rightarrow \mathcal{L}_m \left(\sum_{k=1}^{M_p} x_k b_k \right) = 0 \quad \forall m \\ &\Rightarrow \sum_{k=1}^{M_p} x_k b_k = \mathbf{0} \Rightarrow \mathbf{x} = \mathbf{0}, \end{aligned} \quad (27)$$

which, with linearity, establishes the invertibility of \mathbf{L} . The same strategy shows the invertibility of $\tilde{\mathbf{L}}$. We now have

$$\mathbf{A} = \mathbf{A} \Rightarrow \tilde{\mathbf{A}} \tilde{\mathbf{L}} \tilde{\mathbf{L}}^{-1} = \mathbf{A} \mathbf{L} \mathbf{L}^{-1} \Rightarrow \tilde{\Sigma}_p \tilde{\mathbf{L}}^{-1} = \Sigma_p \mathbf{L}^{-1} \quad (28)$$

from which we obtain the looked for relationship

$$\tilde{\Sigma}_p = \Sigma_p \mathbf{M} \quad (29)$$

with $\mathbf{M} = \mathbf{L}^{-1} \tilde{\mathbf{L}}$, an invertible matrix. \square

The well-posedness of the definition of the projectors in (22) and (23) now follows. In particular

Corollary 1. *The quasi-Helmholtz projectors are invariant on any specific choice of an high-order Star matrix satisfying (19).*

Proof. Given two matrices as above, we have from the previous proposition that $\tilde{\Sigma}_p = \Sigma_p \mathbf{M}$ with \mathbf{M} unique and invertible. First note that, letting

$$\Sigma_p = \mathbf{U} \mathbf{S} \mathbf{V}^T \quad (30)$$

be the reduced Singular Value Decomposition (SVD) of Σ (i.e. the SVD where \mathbf{U} and \mathbf{V} are vertically rectangular and column full rank matrices), then

$$\mathbf{M}^T \Sigma_p^T \Sigma_p \mathbf{M} = \left(\mathbf{M}^T \mathbf{V} \mathbf{S}^T \right) \left(\mathbf{S} \mathbf{V}^T \mathbf{M} \right) \quad (31)$$

where the left matrix in parenthesis is a full column rank matrix and the right matrix in parenthesis is a full row rank matrix. By using the properties of pseudoinverses [22] we get

$$\left(\mathbf{M}^T \Sigma_p^T \Sigma_p \mathbf{M} \right)^+ = \left(\mathbf{S} \mathbf{V}^T \mathbf{M} \right)^+ \left(\mathbf{M}^T \mathbf{V} \mathbf{S}^T \right)^+ \quad (32)$$

from which it follows that

$$\begin{aligned} \mathbf{P}_p^{\tilde{\Sigma}} &= \tilde{\Sigma}_p \left(\tilde{\Sigma}_p^T \tilde{\Sigma}_p \right)^+ \tilde{\Sigma}_p^T \\ &= \Sigma_p \mathbf{M} \left(\mathbf{M}^T \Sigma_p^T \Sigma_p \mathbf{M} \right)^+ \mathbf{M}^T \Sigma_p^T \\ &= \mathbf{U} \mathbf{S} \mathbf{V}^T \mathbf{M} \left(\mathbf{S} \mathbf{V}^T \mathbf{M} \right)^+ \left(\mathbf{M}^T \mathbf{V} \mathbf{S}^T \right)^+ \mathbf{M}^T \mathbf{V} \mathbf{S}^T \mathbf{U}^T \\ &= \mathbf{U} \mathbf{U}^T = \Sigma_p \left(\Sigma_p^T \Sigma_p \right)^+ \Sigma_p^T = \mathbf{P}_p^{\Sigma}. \end{aligned} \quad (33)$$

The uniqueness of \mathbf{P}_p^{Σ} combined with (23) directly implies that of $\mathbf{P}_p^{\Lambda H}$. \square

B. Projector Based Solution to the Low Frequency Breakdown

To fix ideas and obtain an algorithm for the projectors, we propose to choose the following explicit definition of the Star matrix Σ_p [17]

$$\left[\Sigma_p^T \right]_{mn} = \int_{\Gamma} \sigma_m^{(p)}(\mathbf{r}) \nabla_{\Gamma} \cdot \boldsymbol{\psi}_n^{(p)}(\mathbf{r}) dS(\mathbf{r}) \quad (34)$$

where the functions $\sigma_m^{(p)}$ are defined in (8). The reader should note that this definition results in a standard Star matrix in the zeroth-order ($p = 0$) case and generalizes the concept for higher orders. Other choices however could have been made without modifying the final results, as proved above. Now, from (24), the high-order quasi-Helmholtz projectors satisfy

$$\mathbf{P}_p^{\Lambda H} \mathbf{T}_h = \mathbf{0} \quad \text{and} \quad \mathbf{T}_h \mathbf{P}_p^{\Lambda H} = \mathbf{0}, \quad (35)$$

which generalizes the analogous property valid in the zeroth-order case [9]. This allows to proceed with the same formal strategy developed for zeroth-order projectors that here will work for the high-order EFIE. Define the preconditioning matrix

$$\mathbf{P} = j \sqrt{k/C} \mathbf{P}_p^{\Sigma} + \sqrt{C/k} \mathbf{P}_p^{\Lambda H}, \quad (36)$$

with the scaling factor

$$C = \sqrt{\frac{\|\mathbf{T}_h\|}{\|\mathbf{P}_p^{\Lambda H} \mathbf{T}_s \mathbf{P}_p^{\Lambda H}\|}}. \quad (37)$$

The preconditioned system reads

$$\mathbf{P} \mathbf{T} \mathbf{P} \mathbf{y} = \mathbf{P} \mathbf{e}, \quad (38)$$

with

$$\mathbf{j} = \mathbf{P} \mathbf{y}. \quad (39)$$

The proof of low-frequency well-conditioning and stability of (38) is formally identical to the one for the zeroth-order case [9] and we omit it here for the sake of conciseness.

IV. IMPLEMENTATION RELATED DETAILS

In this section, we deal with implementation related details that could be useful to the reader while implementing all new techniques described here.

We assume that all matrix-vector products are done in a quasi-linear number of operations, using a compression approach [23], [24] for the integral operators and a sparse algorithm for the Star matrices. Note that, to match the computational complexity of fast matrix-vector product algorithms, the naive computation of the norms in (37) should be avoided and iterative approaches, such as power iterations [25], should be used instead. Moreover, the numerical (pseudo-)inversion of $\Sigma_p^T \Sigma_p$ in (22) has to be done iteratively whenever a product with the projectors is involved. As in the zeroth-order case, this matrix is similar to the one we get by discretizing the Laplacian equation with finite elements of order p . We can thus rely on algorithms tailored to solve such systems from other fields of applications [26]. In particular, multigrid algorithms have proven to be quite effective. Because there exists several variants of multigrids, one could use the p -multigrid versions [26]–[28] (tailored for high-order finite elements) but

there are also robust implementations of the standard algebraic multigrid [29] generalized to different scenarios that are often easier to use in a black-box fashion.

Finally, to maximize the effect of our regularization to all frequencies, the computation of the projected EFIE has to be done carefully. For numerical purposes, the cancellations (35) are to be enforced explicitly in the computation of the preconditioned matrix [9], which reads

$$\begin{aligned} \mathbf{PTP} = & jC \mathbf{P}_p^{\Delta H} \mathbf{T}_s \mathbf{P}_p^{\Delta H} + j/C \mathbf{T}_h - k \mathbf{P}_p^{\Delta H} \mathbf{T}_s \mathbf{P}_p^{\Sigma} \\ & - k \mathbf{P}_p^{\Sigma} \mathbf{T}_s \mathbf{P}_p^{\Delta H} - jk^2/C \mathbf{P}_p^{\Sigma} \mathbf{T}_s \mathbf{P}_p^{\Sigma}. \end{aligned} \quad (40)$$

The loss of significant digits in the computation of the right-hand side also has to be avoided, as is well-known when dealing with very low-frequency numerical strategies [9]. In particular, the solenoidal and non-solenoidal contributions of the right-hand side must be computed separately, and the static part of the excitation source is subtracted when tested with the solenoidal functions [9], [11]. More explicitly, we write

$$\mathbf{P}e = j\sqrt{k/C} \mathbf{P}_p^{\Sigma} e + \sqrt{C/k} \mathbf{P}_p^{\Delta H} e_{\text{sub}}, \quad (41)$$

where e_{sub} is the subtracted right-hand side [9]. Finally, the post-processing computation of the electric field requires a similar treatment, by using separately the solenoidal and non-solenoidal contributions of the solution

$$\mathbf{j}_{\text{sol}} = \sqrt{C/k} \mathbf{P}_p^{\Delta H} \mathbf{y} \quad \text{and} \quad \mathbf{j}_{\text{nsol}} = j\sqrt{k/C} \mathbf{P}_p^{\Sigma} \mathbf{y} \quad (42)$$

and subtracting the static part of the Green's kernel when integrating with the solenoidal contribution [9].

V. NUMERICAL VALIDATION

In this section, we give numerical results that validate the use of the quasi-Helmholtz projectors by comparing it against the standard EFIE and against a standard quasi-Helmholtz decomposition. The quasi-Helmholtz decomposition we adopted for comparison is a generalization of the Loop/Star technique (L/S-EFIE) from the zeroth-order: the matrix Σ_p is used for generating the Stars and the Loops are computed as described in [14]. The meshes are generated from the software Gmsh that provides quadratic (curvilinear) triangles [30]. The singular integrals are computed using the singularity cancellation scheme described in [3] while near-singular and far interactions are computed with Gaussian quadratures.

Our first validation is done over the unitary sphere for different frequencies. Figure 1 shows the condition number of system matrix for each different method as a function of frequency and for different orders. We observe that the condition number of the standard EFIE increases dramatically, as expected, while it remains constant for the standard Loop/Star technique and for the approach proposed here based on high-order quasi-Helmholtz projectors. For the latter case, however, the condition number is lower. This effect can be better understood from the test in Figure 2 where the condition number is shown in function of the inverse mesh size. It is clear that, differently from standard Loop/Star, the new projectors do not worsen the spectral behavior of the original EFIE generalizing what happens in the zeroth-order case [9]. The radar cross sections (RCS) at 100Hz and at 3×10^8 Hz

are obtained in Figures 3 and 4, respectively. This shows that the low frequency-breakdown, absent at higher frequencies, is instead corrupting the results at low-frequency when no low-frequency treatment is employed. At the same time, these results validate the stability of our scheme in a wide frequency range.

To test the performance of our scheme on a non-simply connected geometry we used the ‘‘two interlocked M3bius ring’’ structure, that form two separate objects with interlaced holes and handles. The rings are of radius 1m and are discretized with 3780 cells and 5670 edges. In total, there are 72 global Loops associated with this topology. Figure 5 shows the surface density current obtained by solving the EFIE with and without preconditioning at 10Hz using basis functions of order two (39690 unknowns). We get, without the need of detecting the global Loops, the same results with the quasi-Helmholtz projectors and the Loop/Star-EFIE for which however the global Loops must be explicitly detected. It should also be noted that the accuracy is completely lost without preconditioning.

Our final validation test scenario is on the model of an airliner with 2D apertures corresponding to the windows and the shell of the jet engine. The mesh contains 3942 cells and 5750 internal edges, and we use basis functions of order two (42900 unknowns). In addition to show the relevance of our method to solve industrial scenarios, this example completes the numerical study with problems containing global Loops around apertures, which are of different kind than the harmonic Loops of the previous example. Figure 6 shows the surface density current obtained by solving the EFIE with and without preconditioning at 1Hz. As for the previous case, the quasi-Helmholtz projectors give an identical solution as the one obtained with Loop-Star decompositions (which however requires Loop detection), while the solution without preconditioning is completely jeopardized.

VI. CONCLUSION

In this work, we have extended the use of the quasi-Helmholtz projectors for stabilizing the EFIE when discretized with high-order basis functions. The new scheme is based on a generalized definition of Star matrix that is wide enough to encompass numerous relevant scenarios, including the use of GWP basis elements. The contribution has shown that this results into unique quasi-Helmholtz projectors irrespectively of the specific choice of Star matrix. Numerical results has shown the effectiveness of the new approach.

ACKNOWLEDGMENT

The work of this paper has received funding from the EU H2020 research and innovation programme under the Marie Skłodowska-Curie grant agreement n^o 955476 (project COM-PETE), from the European Research Council (ERC) under the European Union's Horizon 2020 research and innovation programme (grant agreement n^o 724846, project 321).

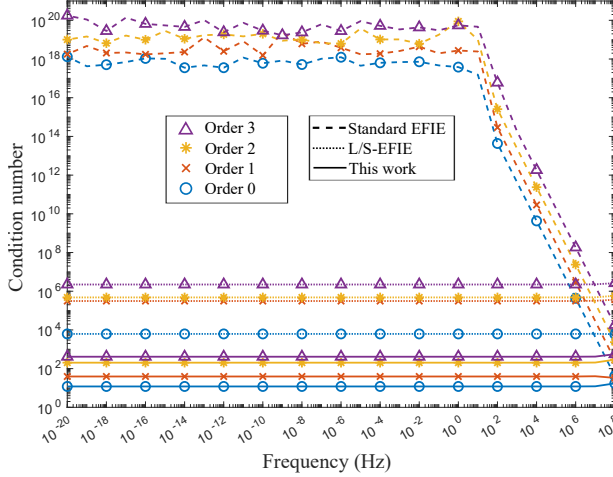


Fig. 1. Condition number of the system matrices in function of the frequency for order zero to three.

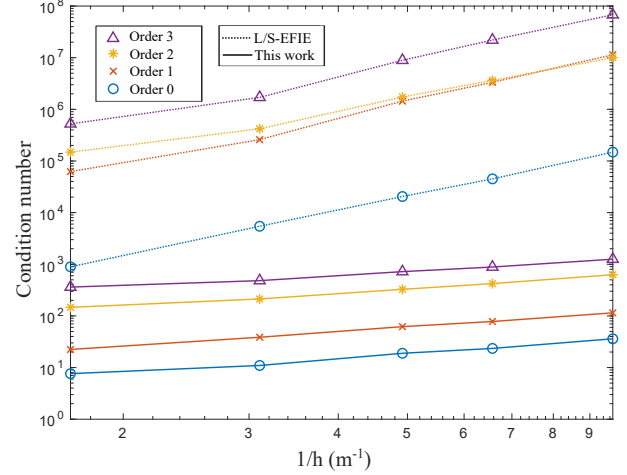


Fig. 2. Condition number of the system matrices in function of the inverse of the average cell diameter h ; frequency of 1Hz.

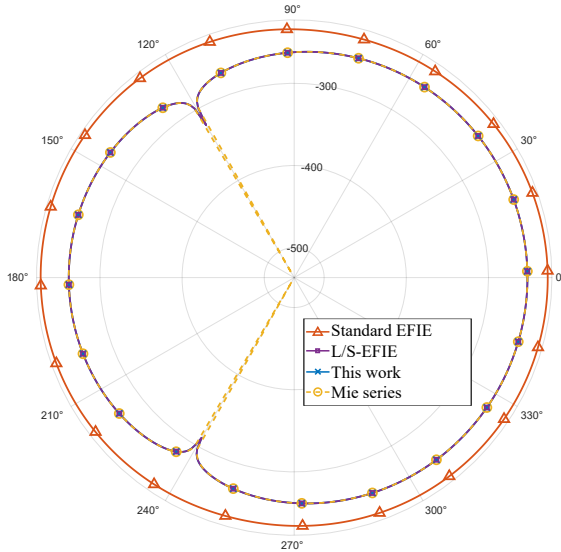


Fig. 3. Radar cross section (RCS) in dBsm at 100Hz.

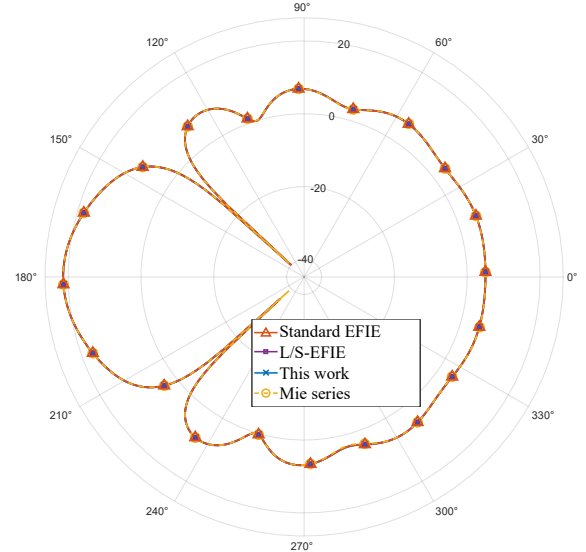


Fig. 4. Radar cross section (RCS) in dBsm at 3×10^8 Hz.

REFERENCES

- [1] W. C. Chew, E. Michielssen, J. Song, and J. Jin, *Fast and Efficient Algorithms in Computational Electromagnetics*. Artech House, 2001.
- [2] W. C. Gibson, *The method of moments in Electromagnetics*. Champan & Hall/CRC Press, 2021.
- [3] S. Sauter and C. Schwab, *Boundary Element Methods*, ser. Springer Series in Computational Mathematics. Springer Berlin Heidelberg, 2010.
- [4] S. M. Rao, D. R. Wilton, and A. W. Glisson, "Electromagnetic scattering by surfaces of arbitrary shape," *IEEE Transactions on Antennas and Propagation*, vol. 30, no. 3, pp. 409–418, 1982.
- [5] R. Graglia, D. Wilton, and A. Peterson, "Higher order interpolatory vector bases for computational electromagnetics," *IEEE Transactions on Antennas and Propagation*, vol. 45, no. 3, pp. 329–342, Mar. 1997, conference Name: IEEE Transactions on Antennas and Propagation.
- [6] R. D. Graglia and A. F. Peterson, *Higher-Order Techniques in Computational Electromagnetics*. Edison, NJ: Scitech Publishing, Nov. 2015.
- [7] M. Djordjevic and B. Notaras, "Double higher order method of moments for surface integral equation modeling of metallic and dielectric antennas and scatterers," *IEEE Transactions on Antennas and Propagation*, vol. 52, no. 8, pp. 2118–2129, Aug. 2004, conference Name: IEEE Transactions on Antennas and Propagation.
- [8] A. Peterson and M. Bibby, "Error trends in higher-order discretizations of the EFIE and MFIE," in *2005 IEEE Antennas and Propagation Society International Symposium*, vol. 3A, 2005, pp. 52–55 vol. 3A.
- [9] S. B. Adrian, A. Dély, D. Consoli, A. Merlini, and F. P. Andriulli, "Electromagnetic Integral Equations: Insights in Conditioning and Preconditioning," *IEEE Open Journal of Antennas and Propagation*, vol. 2, pp. 1143–1174, 2021.
- [10] G. Vecchi, "Loop-star decomposition of basis functions in the discretization of the EFIE," *IEEE Transactions on Antennas and Propagation*, vol. 47, pp. 339–346, 1999.
- [11] J.-S. Zhao and W. C. Chew, "Integral equation solution of Maxwell's equations from zero frequency to microwave frequencies," *IEEE Transactions on Antennas and Propagation*, vol. 48, no. 10, pp. 1635–1645, 2000.
- [12] J.-F. Lee, R. Lee, and R. Burkholder, "Loop star basis functions and a robust preconditioner for EFIE scattering problems," *IEEE Transactions on Antennas and Propagation*, vol. 51, no. 8, pp. 1855–1863, 2003.
- [13] T. Eibert, "Iterative-solver convergence for loop-star and loop-tree decompositions in method-of-moments solutions of the electric-field

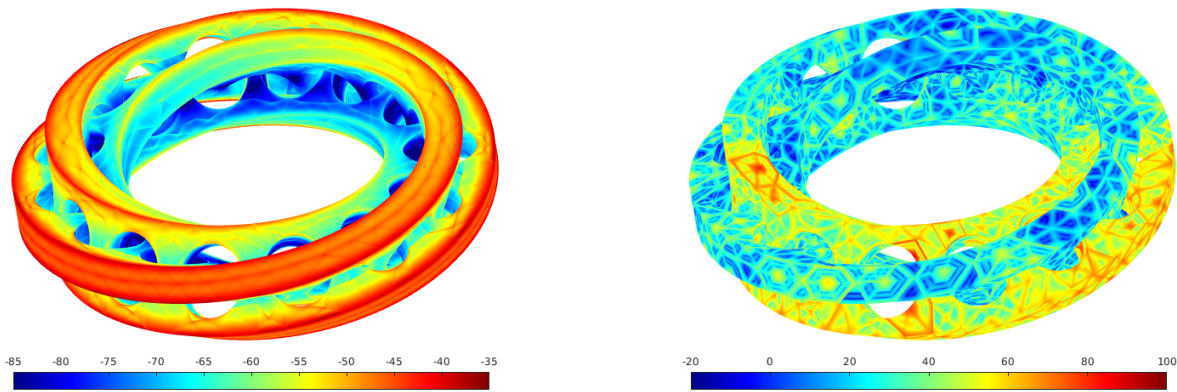


Fig. 5. Absolute value of the surface density current (in dB_{A/m^2}) for the interlocked Möbius ring irradiated by a plane wave at 10Hz, with preconditioning (up) and without (down).

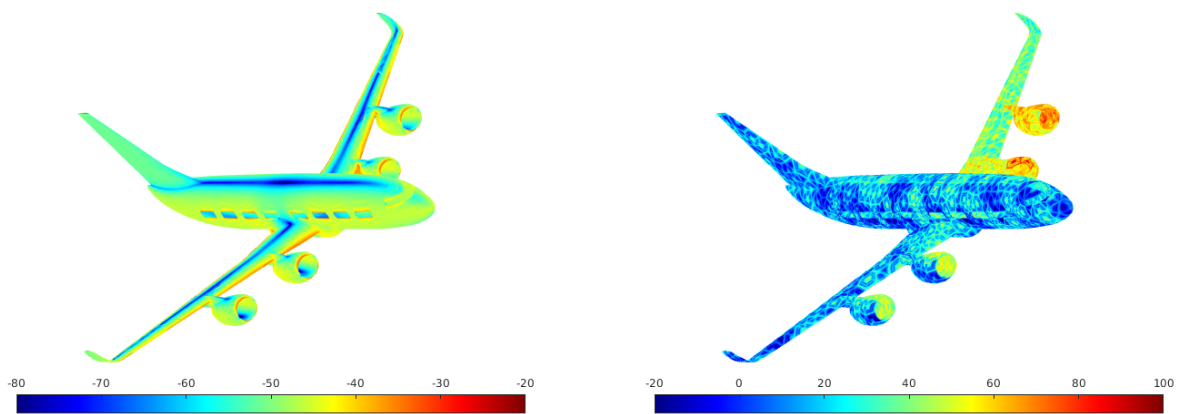


Fig. 6. Absolute value of the surface density current (in dB_{A/m^2}) for the airliner irradiated by a plane wave at 1Hz, with preconditioning (left) and without (right).

- integral equation," *IEEE Antennas and Propagation Magazine*, vol. 46, no. 3, pp. 80–85, 2004.
- [14] R. Wildman and D. Weile, "An accurate broad-band method of moments using higher order basis functions and tree-loop decomposition," *IEEE Transactions on Antennas and Propagation*, vol. 52, no. 11, pp. 3005–3011, Nov. 2004, conference Name: IEEE Transactions on Antennas and Propagation.
- [15] F. Valdés, F. P. Andriulli, K. Cools, and E. Michielssen, "High-order Div- and Quasi Curl-Conforming Basis Functions for Calderón Multiplicative Preconditioning of the EFIE," *IEEE Transactions on Antennas and Propagation*, vol. 59, no. 4, pp. 1321–1337, Apr. 2011, conference Name: IEEE Transactions on Antennas and Propagation.
- [16] J. Bourhis, A. Merlini, and F. Andriulli, "High-order quasi-Helmholtz Projectors: Definition, Analyses, Algorithms," in *XXXVth General Assembly and Scientific Symposium of the International Union of Radio Science*, 2023.
- [17] A. Merlini, "Unified computational frameworks bridging low to high frequency simulations: fast and high fidelity modelling from brain to radio-frequency scenarios," Ph.D. dissertation, Ecole nationale supérieure Mines-Télécom Atlantique, 2019.
- [18] A. Peterson, "Mapped Vector Basis Functions for Electromagnetic Integral Equations," *Synthesis Lectures on Computational Electromagnetics*, vol. 1, pp. 1–124, 12 2005.
- [19] J. Nédélec, "Mixed Finite Elements in \mathbb{R}^3 ." *Numerische Mathematik*, vol. 35, pp. 315–342, 1980. [Online]. Available: <http://eudml.org/doc/186293>
- [20] D. Boffi, F. Brezzi, and M. Fortin, *Mixed Finite Element Methods and Applications*. Springer Berlin, Heidelberg, 2013.
- [21] B. M. Notaros, "Higher Order Frequency-Domain Computational Electromagnetics," *IEEE Transactions on Antennas and Propagation*, vol. 56, no. 8, pp. 2251–2276, Aug. 2008, conference Name: IEEE Transactions on Antennas and Propagation.
- [22] A. Ben-Israel and T. N. Greville, *Generalized inverses: theory and applications*. Springer Science & Business Media, 2003, vol. 15.
- [23] X.-M. Pan, L. Cai, and X.-Q. Sheng, "An efficient high order multi-level fast multipole algorithm for electromagnetic scattering analysis," *Progress In Electromagnetics Research*, vol. 126, pp. 85–100, 2012.
- [24] S. Rjasanow and L. Weggler, "ACA accelerated high order BEM for Maxwell problems," *Computational Mechanics*, vol. 51, 04 2013.
- [25] G. W. Stewart, "A Krylov–Schur Algorithm for Large Eigenproblems," *SIAM Journal on Matrix Analysis and Applications*, vol. 23, no. 3, pp. 601–614, 2002. [Online]. Available: <https://doi.org/10.1137/S0895479800371529>
- [26] B. Helenbrook, D. Mavriplis, and H. Atkins, "Analysis of "p"-Multigrid for Continuous and Discontinuous Finite Element Discretizations," *16th AIAA Computational Fluid Dynamics Conference*, 06 2003.
- [27] R. Tielen, M. Möller, D. Göddeke, and C. Vuik, "p-multigrid methods and their comparison to h-multigrid methods within Isogeometric Analysis," *Computer Methods in Applied Mechanics and Engineering*, vol. 372, p. 113347, 2020.
- [28] I. Huisman, J. Stiller, and J. Fröhlich, "Scaling to the stars – a linearly scaling elliptic solver for p-multigrid," *Journal of Computational Physics*, vol. 398, p. 108868, 2019.
- [29] A. Napov and Y. Notay, "Algebraic multigrid for moderate order finite elements," *SIAM Journal on Scientific Computing*, vol. 36, no. 4, pp. A1678–A1707, 2014. [Online]. Available: <https://doi.org/10.1137/130922616>
- [30] Geuzaine, Christophe and Remacle, Jean-Francois, "Gmsh." [Online]. Available: <http://http://gmsh.info/>